

Clear-sky aerosol optical depth over East China estimated from visibility measurements and chemical transport modeling



Jintai Lin ^{a,*}, Aaron van Donkelaar ^b, Jinyuan Xin ^c, Huizheng Che ^d, Yuesi Wang ^c

^a Laboratory for Climate and Ocean-Atmosphere Studies, Department of Atmospheric and Oceanic Sciences, School of Physics, Peking University, Beijing, 100871, China

^b Department of Physics and Atmospheric Science, Dalhousie University, Halifax, Canada

^c State Key Laboratory of Atmospheric Boundary Layer Physics and Atmospheric Chemistry, Institute of Atmospheric Physics, Chinese Academy of Sciences, Beijing, 100029, China

^d Key Laboratory of Atmospheric Chemistry (LAC), Institute of Atmospheric Composition, Chinese Academy of Meteorological Sciences (CAMS), CMA, Beijing, 100081, China

HIGHLIGHTS

- We use chemical transport modeling to improve conversion from visibility to AOD.
- We use MODIS and three ground AOD networks to validate visibility-inferred AOD.
- Seasonal and daytime variations of visibility-inferred AOD agree with MODIS AOD.
- Our visibility-based AOD inference can be used for multi-decadal aerosol studies.

ARTICLE INFO

Article history:

Received 25 January 2014

Received in revised form

23 May 2014

Accepted 19 June 2014

Available online 20 June 2014

Keywords:

Visibility

Aerosol optical depth

Chemical transport model

Seasonal variation

Daytime variation

China

ABSTRACT

Horizontal visibility measured at ground meteorological stations provides an under-exploited source of information for studying the interdecadal variation of aerosols and their climatic impacts. Here we propose to use a 3-hourly visibility dataset to infer aerosol optical depth (AOD) over East China, using the nested GEOS-Chem chemical transport model to interpret the spatiotemporally varying relations between columnar and near-surface aerosols. Our analysis is focused in 2006 under cloud-free conditions. We evaluate the visibility-inferred AOD using MODIS/Terra and MODIS/Aqua AOD datasets, after validating MODIS data against three ground AOD measurement networks (AERONET, CARSNET and CSHNET). We find that the two MODIS datasets agree with ground-based AOD measurements, with negative mean biases of 0.05–0.08 and Reduced Major Axis regression slopes around unity. Visibility-inferred AOD roughly capture the general spatiotemporal patterns of the two MODIS datasets with negligible mean differences. The inferred AOD reproduce the seasonal variability (correlation exceeds 0.9) and the slight AOD growth from the late morning to early afternoon shown in the MODIS datasets, suggesting the validity of our AOD inference method. Future research will extend the visibility-based AOD inference to study the long-term variability of AOD.

© 2014 The Authors. Published by Elsevier Ltd. This is an open access article under the CC BY-NC-ND license (<http://creativecommons.org/licenses/by-nc-nd/3.0/>).

1. Introduction

Climate forcings of aerosols are among the most uncertain aspects in climate change studies. Due to their relatively short lifetimes, aerosols undergo significant spatial and temporal variability, and are highly dependent on emissions, atmospheric formation, transport, and removal processes. The spatiotemporal variability

also means that a large amount of measurements with good coverage in space and time are required to constrain their climatic impacts. Such measurements are rare before the 21st century, especially over developing countries like China. Previous studies have suggested that aerosols may have significantly affected surface air temperature (Qian and Giorgi, 2000) and precipitation (Qian et al., 2009) over various parts of China. A reliable dataset for historical aerosols would provide additional insight into these impacts.

Near-surface horizontal visibility has been measured routinely at many ground meteorological stations for many decades. Given

* Corresponding author.

E-mail address: linjt@pku.edu.cn (J. Lin).

the impairment of light by aerosols, visibility measurements can be used to infer aerosol optical effects after constraining the effects of non-aerosol factors like air molecules and hydrometeors (Griffing, 1980; Husar et al., 2000; Qian and Giorgi, 2000; Doyle and Dorling, 2002; Vautard et al., 2009; Wang et al., 2012). Previous studies have attempted to convert daily mean or early afternoon visibility to aerosol optical depth (AOD), a key optical characteristic of aerosols in the whole atmospheric column (Qiu and Lin, 2001; Chen et al., 2009b; Wang et al., 2009; Qin et al., 2010). In converting visibility to AOD, these studies have normally assumed an exponential decrease of aerosols with height, with a scale height of 0.8–1.2 km that depends linearly and weakly on visibility (Elterman, 1970). Qiu and Lin (2001) proposed a correction on the vertical profile based on near-surface water vapor pressure. Nonetheless, the simplified conversion approach cannot fully account for the large variability with space and time in the aerosol vertical profile (van Donkelaar et al., 2013; Yang et al., 2013). For example, the vertical shape of aerosols are often not exponential (Liu et al., 2011), and in the downwind regions the free tropospheric aerosols play a much more important role than suggested by the exponential profile (Ford and Heald, 2012). There is also significant variability in vertical mixing in the planetary boundary layer (PBL), with the PBL height varying diurnally and day-to-day by up to an order of magnitude (Lin et al., 2008, 2012; Yang et al., 2013).

In this study, we propose to use a 3-hourly visibility dataset for AOD inference over East China (see Fig. 1 for domain definition). To relate near-surface to columnar aerosols, we employ the vertical profiles of aerosols simulated by the nested GEOS-Chem chemical transport model (CTM). Driven by assimilated meteorology, the model accounts for the horizontal and temporal (hourly, daily and seasonal) variations of aerosol profiles. The model profiles have been used to convert satellite AOD data to near-surface PM_{2.5} mass concentrations (van Donkelaar et al., 2010, 2013) and visibility (Kessner et al., 2013). Similar modeling approaches have been adopted for studying trace gases (Lamsal et al., 2008; Lin et al., 2010). In addition, the use of 3-hourly data allows for an analysis of AOD variability during the daytime, an important aspect for the climatic impacts of aerosols. Although the diurnal variation of AOD is likely small on the annual and global scale (Kaufman et al., 2000; Ichoku et al., 2005), the range of variation depends on season, the

magnitude of AOD, and the contribution of anthropogenic sources (Kaufman et al., 2000; Wang et al., 2010).

Visibility-inferred AOD are subject to errors in visibility data, influences by non-aerosol factors, and assumptions in the conversion process from visibility to AOD. We thus evaluate the inferred data using independent AOD data from the Moderate Resolution Imaging Spectroradiometer (MODIS) onboard the Terra and Aqua satellites and from three ground networks including the Aerosol Robotic Network (AERONET), the China Aerosol Remote Sensing Network (CARSNET), and the Chinese Sun Hazemeter Network (CSHNET) (see Fig. 1 for locations of the individual stations). Considering that ground stations for AOD measurements are not collocated with stations for visibility observations and that there are much fewer AOD stations, we use ground-based AOD measurements to validate MODIS data and then use MODIS data to evaluate visibility-inferred AOD. Such ‘transfer evaluation’ maximizes the use of ground-measured and MODIS AOD data. Our analysis is focused in 2006 under cloud-free conditions, concerning the measurement conditions for MODIS and ground AOD networks as well as the data availability in CARSNET and CSHNET (both available for 2006).

Section 2 presents AOD data from MODIS and ground networks, visibility data, GEOS-Chem simulations, and the method to converting visibility to AOD. Section 3 compares MODIS AOD to those from the ground networks. Section 4 evaluates visibility-inferred AOD using MODIS AOD data, focusing on the spatial, seasonal, and daytime hourly variations. Section 5 summarizes the paper.

2. Data, modeling and methodology

2.1. AOD measurements from three ground networks

Fig. 1 shows the distribution of three ground networks over East China. AERONET is a world-renowned remote sensing aerosol monitoring network (Holben et al., 1998). It has been used previously to provide aerosol optical properties (Liu et al., 2007) for the derivation and/or evaluation of satellite remote sensing or atmospheric modeling of aerosols (Mi et al., 2007; van Donkelaar et al., 2013; Lin et al., 2014). However, AERONET includes few sites in China with continuous aerosol measurements, affecting its regional representativeness in various applications. The network provides level-2 (quality-assured) AOD data at the wavelengths of 440 nm, 675 nm, 870 nm and 1020 nm; these data have been subject to both automatic and manual cloud screening. In this study, AOD data at 550 nm at four stations are derived from values at 440 nm using the accompanying Ångström exponent data for 440–675 nm.

Operated by the China Meteorological Administration since 2002, CARSNET is the Chinese version of AERONET designed for studying aerosol optical properties in different areas of China (Che et al., 2009). The network uses the same CE-318 sun photometers as in AERONET. The CARSNET instruments undergo the Langley calibration at the Izana Observatory (INM, Spain), following the protocol used by AERONET. An instrument inter-comparison calibration is also conducted at the Chinese Academy of Meteorological Sciences (CAMS) site (Che et al., 2009, 2013). In addition, sphere calibration is performed every year to ensure the accuracy of the sky irradiance measurement (Tao et al., 2013). CARSNET provides both level 1.0 (raw AOD without cloud screening) and level-1.5 AOD (cloud-screened AOD based on the work of (Smirnov et al. (2000)) products using the ASTPwin software offered by Cimel Ltd. Co. AOD data are available at 440 nm, 670 nm, 870 nm and 1020 nm, together with the Ångström exponent calculated from AOD values at 440 nm and 870 nm. The CARSNET level-1.5 data at the CMAS site agree with the AERONET/PHOTONS level-1.5 data (Che et al., 2009; Pan et al., 2010). The CARSNET dataset

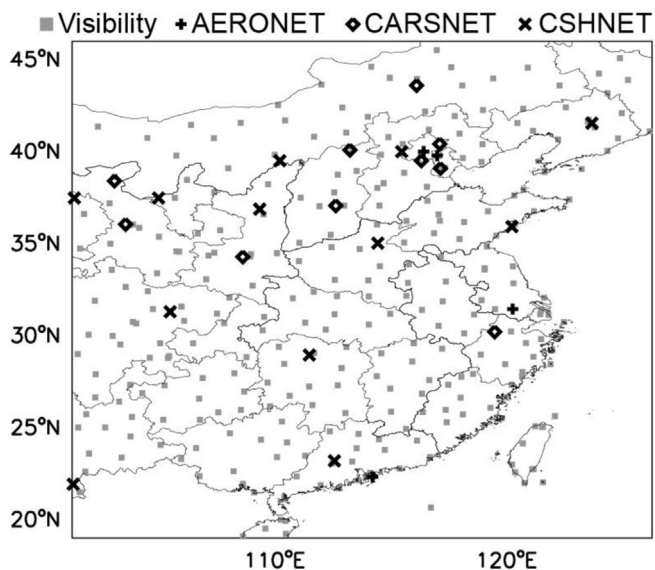


Fig. 1. Stations of visibility measurements and three ground AOD networks over East China.

has been employed to evaluate MODIS Collection 5 AOD products over many regions of China (Pan et al., 2010; Xie et al., 2011). In this study, we calculate the level-1.5 CARSNET AOD at 550 nm at 10 stations using AOD at 440 nm and the accompanying Ångström exponent data.

Established in 2004 by the Institute of Atmospheric Physics, CSHNET implements handheld sun hazemeters to measure aerosol optical properties across the ecologically diverse areas of China (Xin et al., 2007). Measurements are conducted in the morning and afternoon close to the overpass times of polar orbiting satellites carrying aerosol measurement instruments (e.g., MODIS). AOD data are provided at four spectral channels: 405 nm, 500 nm, 650 nm, and 880 nm. Ångström exponent is derived with log linear fitting using AOD values at 405 nm, 500 nm and 650 nm. Cloud screening is done manually by the observers holding the photometers. The hazemeters are calibrated annually with a CE-318 sun photometer at Xianghe as part of AERONET. Additional periodic calibration is performed through the Langley method for selected photometers and through transfer calibration for the rest photometers (Xin et al., 2007). Calibration for February–August 2005 showed that the hazemeter AOD data at 405 nm, 500 nm and 650 nm are generally within 2%–6% of the CE-318 photometer results. CSHNET data have been compared with MODIS Collection 4 and 5 AOD products over China (Li et al., 2007; Wang et al., 2007, 2010) and MODIS Collection 5.1 product around the Bohai Sea area (Xin et al., 2011). In this study, we use CSHNET AOD at 500 nm and associated Ångström exponent data to derive AOD values at 550 nm at 12 stations.

2.2. MODIS AOD data retrieved from Terra and Aqua

We use the Collection 5.1 level 2 products MOD04 and MYD04 (Levy et al., 2007) retrieved from the Terra and Aqua satellites, respectively. Following Hyer et al. (2011), we strengthen the data selection criteria to enhance data quality. We only include MODIS data under clear-sky conditions (cloud fraction = 0) with the ‘very good’ quality assurance flag and with scattering angle less than 170°. We screen out scenes with potential problems in surface reflectance, based on the MODIS MCD43C3 albedo product. We remove scenes with non-zero snow fraction within 0.175° of the scene centers. We exclude data when surface albedo exceeds 0.08 at 480 nm, 0.17 at 650 nm or 0.33 at 2100 nm, or when surface albedo at 650 nm exceeds 85% of the albedo at 2100 nm; AOD errors increase under these circumstances (Hyer et al., 2011). Hyer et al. (2011) showed that the strengthened data screening generally enhances the consistency between MODIS and AERONET data on a global scale. However, the evaluation over China was limited by the small number of AERONET sites.

2.3. GEOS-Chem simulation

We use the nested GEOS-Chem model for Asia (version 08-03-02; http://wiki.seas.harvard.edu/geos-chem/index.php/Main_Page) (Chen et al., 2009a) to simulate the vertical profile of aerosol extinction coefficient (AEC) for converting near-surface AEC to AOD. Driven by the GEOS-5 assimilation meteorology, the nested model has a horizontal resolution of 0.667° long. × 0.5° lat. with 47 vertical layers. Its lateral boundary conditions of chemicals are taken every 3 h from a global GEOS-Chem simulation at 5° long. × 4° lat. horizontally. The model is run with the standard full gaseous and aerosol chemistry. Aerosols simulated include sulfate–nitrate–ammonium (Park et al., 2004), carbonaceous aerosols (Park et al., 2003), dust (Fairlie et al., 2007) and sea salts (Alexander et al., 2005). Wet deposition of gases and aerosols includes rainout, washout and convective updrafts (Liu et al., 2001), and dry deposition depends on near-surface meteorology and surface

characteristics (Wesely, 1989; Wang et al., 1998). The sulfate–nitrate–ammonium aerosols are simulated with the ISOROPIA-II thermodynamical equilibrium scheme (Fountoukis and Nenes, 2007). Dust particles are emitted with the DEAD scheme (Fairlie et al., 2007), and emissions of sea salts are parameterized by Jaeglé et al. (2011). AOD at 550 nm is calculated from the mass concentration and extinction efficiency for each aerosol type (Drury et al., 2010). Aerosol-type-specific hygroscopic growth of aerosol optical effects is simulated based on the GEOS-5 relative humidity data (Drury et al., 2010). More information on model aerosol optical properties can be found in Drury et al. (2010).

Asian anthropogenic emissions are taken from the INTEX-B dataset (Zhang et al., 2009) for nitrogen oxides (NO_x), carbon monoxide, non-methane volatile organic compounds (VOCs), sulfur dioxide, black carbon and organic carbon. Seasonal dependence of residential emissions follows Lin (2012). Emissions of ammonia are adopted from Streets et al. (2003) with the annual emissions for China scaled to 16.6 Tg (Zhao et al., 2009). Biomass burning emissions are taken from the monthly GFED v2 dataset (van der Werf et al., 2006). Biogenic emissions of VOCs follow MEGAN v2 (Guenther et al., 2006). Soil emissions of NO_x follow Yienger and Levy (1995) and Wang et al. (1998). Lightning emissions of NO_x are parameterized by Price et al. (1997) with a vertical distribution by Ott et al. (2010) and a further budget adjustment according to the OTD/LIS satellite measurements (Murray et al., 2012).

The vertical profile of aerosols is affected by deep convection and PBL mixing, in addition to production and loss processes at different altitudes. In GEOS-Chem, convection is parameterized by a modified Relaxed Arakawa-Schubert scheme (Rienecker et al., 2008), and PBL mixing is parameterized by a non-local scheme driven by the GEOS-5 PBL height (Lin and McElroy, 2010). The GEOS-5 PBL height likely has a negative nighttime bias, and differs from the GEOS-4 height in the daytime (Lin et al., 2012). In the afternoon, the GEOS-5 driven GEOS-Chem generally reproduces the vertical profile of aerosol extinction coefficients retrieved from CALIOP but with a tendency to underestimate aerosols in the free troposphere on a global scale (Ford and Heald, 2012; van Donkelaar et al., 2013). For most of East China, van Donkelaar et al. (2013) showed a summertime underestimate (within 30%) in the afternoon in the modeled ratio of columnar to near-surface (i.e., in the lowest model layer) aerosols.

2.4. Visibility measurements from ground meteorological stations

We adopt the three-hourly visibility data (at 00:00UTC, 03:00UTC, etc.) and other ancillary meteorological parameters from the Integrated Surface Dataset (ISD) from the U.S. National Oceanic and Atmospheric Administration National Climatic Data Center (NCDC) (Smith et al., 2011). This dataset includes ~300 synoptic (non-airport) stations in East China for most years since 1973 with relatively good spatial coverage (Fig. 1). Data from these stations are reported to the World Meteorological Organization via the Global Telecommunications System and, after several processes, finally compiled and archived at NCDC. Of these stations, about 5% were urban sites; currently the non-urban sites are also influenced by air pollution due to urbanization and regional pollution transport. The ISD dataset is processed through 54 quality control algorithms (Lott et al., 2004; Smith et al., 2011). It has been employed to analyze the day-to-day meteorological variation (Lin and McElroy, 2011) and to evaluate the GEOS-5 assimilated meteorology (Lin et al., 2012).

In the daytime, visibility is measured manually as the furthest distance at which the naked eye of an observer can distinguish a predetermined marker object (a building, a mountain, etc.) from the background. The guideline for visibility measurement and recording is given by the China Meteorological Administration

(CMA, 2007) following the World Meteorological Organization recommendation (WMO, 2008). Dark objects are required to ensure the contrast against the background; and objects at as many directions and distances as possible are selected for observation to increase the spatial representativeness of measurements. Visibility measurements are subject to limitations in manual observation (e.g., human mistakes); their spatial representativeness is affected by the presence of plumes and other occasional heterogeneity in the local air. Visibility is recorded as discrete numbers, usually at intervals of 0.1 km for distances within 1 km, of 1 km for distances 1–10 km away, and of 5 km for distances 10–30 km away. Visibility exceeding 30 km is recorded as 30 km. Detailed procedures can be found in CMA (2007) and (WMO, 2008).

Visibility is reduced by scattering/absorption of light by air molecules, hydrometeors (rain, snow, fog, clouds, etc.), and aerosols. Scattering and absorption by air molecules is relatively weak, and visibility below 30 km is caused predominately by the presence of aerosols and hydrometeors. To eliminate the influence of hydrometeors, we remove visibility data when precipitation is observed concurrently. We screen out the times with fog present by eliminating the data when relative humidity exceeds 95%. A threshold at 95% instead of 100% accounts for errors in relative humidity data in the humid environment; using 90% as threshold led to similar results when comparing visibility-inferred AOD to MODIS data. We also remove any visibility data concurrent with ‘ice fog’ and ‘blowing snow’ under cold and windy conditions (Husar et al., 2000).

Upon the quality control protocols embedded in the ISD dataset (Lott, 2004), we perform further data screening to eliminate visibility observations that may be subject to human mistakes, adopting and modifying the procedures by Husar et al. (2000). To eliminate some suspicious data spikes, we exclude days when the daily mean visibility falls below one third of the values in the previous and next day (Husar et al., 2000). We exclude all data at stations where the maximum visibility over the course of 2006 is below 12 km but the median value exceeds 11 km, considering that such lack of variability is often indicative of erroneous data. In addition, we remove the stations where the number of non-repeating visibility values in 2006 is less than five. For comparisons with the clear-sky MODIS AOD, we further remove visibility data when the presence of clouds is reported. Note that our data screening may not fully eliminate erroneous data due to the nature of manual measurement and data recording method.

After the above data screening, coincident visibility data are available under cloud-free conditions at 220 synoptic (non-airport) stations with respect to MODIS/Terra and at 233 stations with respect to MODIS/Aqua; 3% and 5% of the stations are located in the urban areas, respectively. We choose to include the cases with visibility = 30 km because excluding such cases would introduce an undesirable sampling bias affecting later analyses on AOD. In Sect. 2.5, we introduce a correction to compensate for, among other factor, the visibility values being capped at 30 km.

2.5. Conversion from visibility to AOD

In the absence of hydrometeors, the near-surface AEC at 550 nm is inversely proportional to visibility through the Koschmieder Equation if the effect of air molecules is neglected:

$$\text{AEC} = K/V \quad (1)$$

Here V represents visibility and K the Koschmieder constant. The value of K depends on the contrast threshold of the human eye (2–5%) and the optical contrast of the designated marker object against the background. It reaches 3.9 for a human eye contrast

threshold of 2% with optimal contrast between the marker object and the background, and is reduced with weaker contrasts.

As discussed in Sect. 2.4, visibility is recorded as 30 km when exceeding the value. In addition, the relative contribution of scattering/absorption by air molecules enhances with increasing visibility. Errors may also exist in other aspects of manual measurement and data recording. Therefore we modify the AEC-visibility relationship as follows:

$$\text{AEC} = K/V - K/V_0 = K/V*(1 - V/V_0) \quad (2)$$

Here we introduce V_0 to account for the optical effect of air molecules and potential errors in visibility measurements and recording (including but not limited to human errors). For simplicity, we assume that K is not affected by these errors.

For a particular station, the near-surface AEC is converted to AOD at 550 nm using the GEOS-Chem modeled ratio of AOD to AEC, $\text{AOD}_m/\text{AEC}_m$, in the gridcell covering the station:

$$\text{AOD} = \text{AEC}*(\text{AOD}_m/\text{AEC}_m) = K/V*(1 - V/V_0)*(\text{AOD}_m/\text{AEC}_m) \quad (3)$$

Equation (3) corresponds to the conversion formula used by Zhu et al. (2011) and Chen et al. (2013) shown in Eq. (4) below. However, Eq. (3) uses a modeled AOD to near-surface AEC ratio instead of assuming a scale height H (with an implied exponential vertical shape) for aerosols. Equation (3) also uses a different set of values for K and V_0 than Eq. (4) to provide better consistency with MODIS AOD data over East China (see below).

$$\text{AOD} = 3.0/V*(1 - V/205)*H \quad (4)$$

We adopt a maximum value of 3.9 for K (Qiu and Lin, 2001; Chen et al., 2009b; Qin et al., 2010). The value is higher than used in Eq. (4), and compensates for the underestimate in the modeled ratio of columnar to near-surface aerosols (see Sect. 2.3). It contributes to a negligible mean bias in visibility-inferred AOD relative to MODIS data.

The choice of V_0 requires information on errors in visibility measurements and recording procedures that are largely unclear, although the optical effect of air molecules (corresponding to a value at 205 km, as in Eq. (4)) can be quantified straightforwardly. We adopt a value at 70 km to achieve the highest consistency between visibility-inferred and MODIS AOD across the range of AOD values in 2006, after testing various values between 35 km and 110 km for V_0 . For a visibility record at 30 km, the inclusion of $V_0 = 70$ km leads to an ‘effective’ visibility of 52.5 km, an AEC of 0.074 km^{-1} , and thus an AOD averaged at 0.16 around the Terra time and at 0.20 around the Aqua time. The effect of V_0 diminishes rapidly with decreasing values of V . Overall, implementing $V_0 = 70$ km reduces AOD, and the relative effect ranges from –43% for $V = 30$ km to –14% for $V = 10$ km, to –1% for $V = 1$ km, and to within 1% for $V < 1$ km. Using seasonally varying values for V_0 would slightly improve the agreement between inferred and MODIS AOD at the cost of increased algorithm complexity, thus we elect to adopt a single value for V_0 . We note that the estimate of V_0 here is relatively rough, and may be improved by comparisons with MODIS data in multiple years. More analysis of the effect of V_0 is shown in Sect. 4.1.

Another key procedure of our AOD derivation is the use of $\text{AOD}_m/\text{AEC}_m$ ratios. Model simulations have often been used to link columnar to near-surface aerosols (van Donkelaar et al., 2010, 2013; Kessner et al., 2013). van Donkelaar et al. (2013) used GEOS-Chem simulated $\text{AOD}/\text{PM}_{2.5}$ ratios to convert MODIS AOD to near-surface $\text{PM}_{2.5}$ concentrations and achieved significant agreement with in situ measurements over North America (slope = 0.89;

$r = 0.82$). Using GEOS-5 simulations, Kessner et al. (2013) converted MODIS AOD to near-surface AEC and then visibility over the eastern U.S. and found good consistency with visibility measurements (slope = 0.98; $r = 0.70$). Here we use a similar approach to convert near-surface AEC to AOD in the reverse direction.

The choice of AEC_m is not trivial, given the potential bias in the modeled PBL mixing. We find that adopting the modeled AEC from the lowest layer (~130 m thick) results in a mean bias by -20% in the morning-time visibility-inferred AOD relative to MODIS/Terra data. We test the feasibility of an average AEC from multiple model layers, and find that a 6-layer mean AEC (i.e., average in the lowest troposphere 0–800 m above the ground) leads to a bias within 5% in visibility-inferred AOD relative to MODIS/Terra data. Using the 6-layer average AEC (in place of the value in the lowest model layer) affects the afternoon AOD inference insignificantly. This is due to the relatively well mixed PBL in the afternoon simulated by GEOS-Chem. Thus we adopt the 6-layer average AEC from the model to convert visibility to AOD. As such, the chosen AOD_m/AEC_m ratios are about 1.8 ± 1.5 km at the Terra time and 2.4 ± 1.4 km at the Aqua time across the days and stations. We find that using the average AEC within the PBL (Kessner et al., 2013) does not improve the AOD inference.

3. Evaluation of MODIS AOD using ground AOD networks

We first evaluate MODIS AOD over East China using data from the three ground networks. To ensure the spatiotemporal consistency between ground-network and MODIS AOD, we only select MODIS scenes within 0.25° of the ground sites, and average ground-network AOD within 1 h of the local times of MODIS scenes.

Fig. 2 presents the scatter plots of MODIS AOD as a function of ground-network AOD. With respect to both Terra (Fig. 2a) and Aqua (Fig. 2b), there is modest scatter between MODIS and ground-network AOD data, with a correlation coefficient of 0.85. The scatter is largest for AOD values exceeding 0.6, especially for Terra. Selecting ground-network data within 15 min of the MODIS time instead of within 1 h leads to a slight reduction in the scatter with the correlation increasing to 0.87 (not shown).

The Reduced Major-Axis (RMA) regression further shows good agreement between MODIS and ground-network AOD (slope = 1.01, intercept = -0.09 for Terra; and slope = 1.11, intercept = -0.11 for Aqua). On average, MODIS AOD is smaller than ground-network AOD by 0.05–0.08 for both Terra and Aqua. This mainly reflects the underestimate in MODIS AOD in the low-value

cases (Fig. 2a,b). These findings are generally consistent with previous evaluation of MODIS Collection 5 AOD (Mi et al., 2007; Wang et al., 2010).

4. Evaluation of visibility-inferred AOD using MODIS AOD

We then use the strictly screened MODIS Collection 5.1 AOD data to evaluate our visibility-inferred AOD. Section 4.1 analyzes the general characteristics of MODIS and visibility-inferred AOD data in all days from all stations; and Sects. 4.2–4.4 evaluate the spatial, seasonal and daytime hourly variations of visibility-inferred AOD, respectively. Due to the strict cloud screening in Sects. 2.2 and 2.4, the AOD analyzed here represent the cloud-free conditions.

The measured visibility is mostly less than 20 km, a MODIS scene is typically about $10 \text{ km} \times 10 \text{ km}$, and the scene center is not exactly located at the ground station. For spatial consistency, we select MODIS scenes within 0.25° of the ground stations for averaging to derive a value for each day and station. Since visibility and the consequently inferred AOD data have a temporal resolution of 3 h in UTC at any given station, we use piecewise linear interpolation to convert the 3-hourly AOD data to an hourly dataset in local solar time, and then average the inferred AOD data within 1 h of the local times of MODIS scenes. The hourly data are also used to analyze the spatially and annually averaged daytime variation of AOD in Sect. 4.4. Our sensitivity test using cubic spline interpolation gives similar results for comparisons between visibility-inferred and MODIS AOD.

We exclude AOD data exceeding the threshold of 2.0, due to the increased uncertainties in both MODIS and visibility-inferred data. At the high-AOD situations, values of visibility are low and may be subject to larger errors in manual measurement and data recording (as discrete values). MODIS data also contain larger errors when AOD is high, due to the increased difficulty of the satellite instrument to detect throughout the atmosphere (Hyer et al., 2011). Extremely polluted events excluded from the high-AOD threshold here are normally episodic at a scale of days. Implementing the AOD threshold will not significantly affect the use of visibility-inferred AOD data in studying the long-term (e.g., interdecadal) variability and trends of aerosols.

4.1. General characteristics

Fig. 3 shows the frequency of occurrences for clear-sky AOD values within specified bins (0–0.05, 0.05–0.10, etc.), comparing

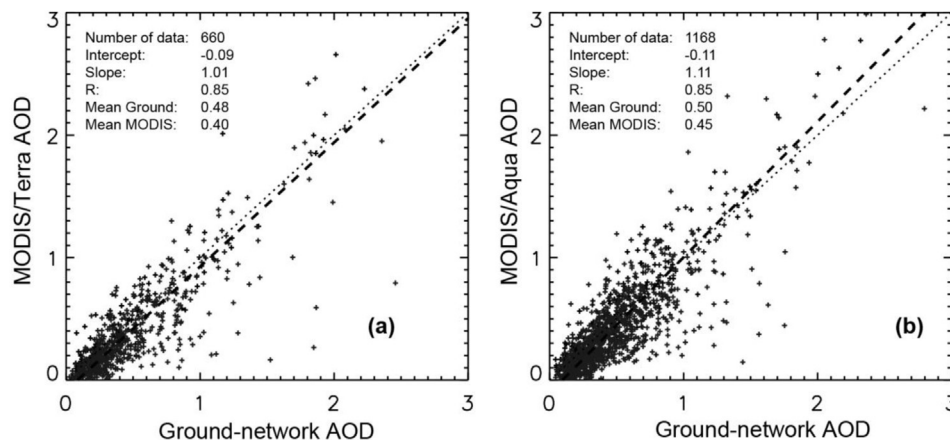


Fig. 2. Scatter plots of MODIS AOD as a function of ground-network AOD over East China. The dashed line depicts the RMA regression and the dotted line indicates the 1:1 relationship. Also shown in each panel are number of data pairs, intercept and slope from the RMA regression, correlation coefficient, and mean AOD from ground networks and MODIS.

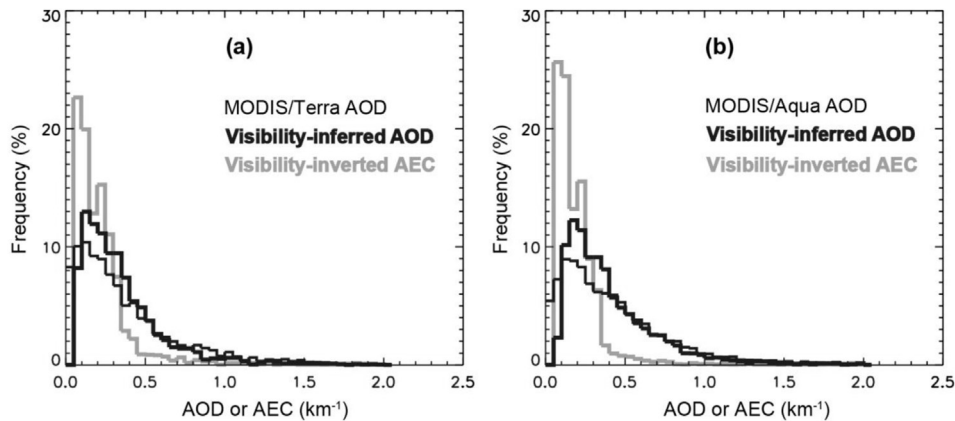


Fig. 3. Frequency of data in individual bins (0–0.05, 0.05–0.10, etc.) for MODIS AOD, visibility-inferred AOD, and visibility-inverted AEC over East China under cloud-free conditions.

MODIS and visibility-inferred data. The frequency distribution has a single mode around 0.1–0.2 for both MODIS/Terra and MODIS/Aqua AOD. The frequency distribution of visibility-inferred AOD roughly resembles that of MODIS, but with more data in the AOD range of 0.1–0.4, much fewer data in the range of 0–0.1, and (particularly in the case of Terra) fewer data for AOD values between 0.6 and 1.2. MODIS/Terra (MODIS/Aqua) AOD are below 0.05 for 8.3% (5.4%) of data points, reflecting the underestimate discussed in Sect. 3. Meanwhile, the inferred AOD is always larger than 0.05, because in the low-aerosol cases (visibility record = 30 km and $AEC = 0.074 \text{ km}^{-1}$) there tend to be more aerosols at higher altitudes than near the surface (i.e., $AOD_m/AEC_m > 1 \text{ km}$). By comparison, the visibility-inverted AEC is concentrated in the range of 0.05–0.35 km^{-1} with few data exceeding 0.35 km^{-1} (Fig. 3). Assuming a fixed vertical profile of AEC would cause the frequency distribution of visibility-inferred AOD to deviate from that of MODIS AOD.

The scatter plots in Fig. 4a,c compare MODIS (*x*-axis) and visibility-inferred AOD (*y*-axis) under cloud-free conditions in all days at all meteorological stations. With respect to both Terra and Aqua, the correlation between MODIS and visibility-inferred AOD exceeds 0.5; the apparent data scatter is related mainly to the spatial patterns discussed in Sect. 4.2. On average, the inferred AOD has a negligible bias (within 0.02) relative to MODIS. The RMA regression slope is about 0.84 with a small positive intercept at 0.04–0.05. The positive intercept persists even if we exclude the cases with visibility recorded at 30 km (the cutoff value). The positive intercept reflects that visibility-inferred AOD are larger than MODIS values in the low-AOD cases, due in part to the underestimate in MODIS AOD discussed in Sect. 3.

The choice of V_0 in Eq. (3) affects the comparisons with MODIS data. Using a value of 205 km instead of 70 km for V_0 would lead to a mean positive bias in the inferred AOD by 0.05 (0.07) relative to MODIS/Terra (MODIS/Aqua). A value of 70 km for V_0 significantly reduces the positive bias in the low-AOD cases due to the cutoff value at 30 km in the visibility records. For the visibility data recorded at 30 km, the inferred AOD are comparable to the respective MODIS AOD with a mean bias within 0.02: the mean MODIS AOD are 0.14 for Terra and 0.19 for Aqua, similar to the values at 0.16 and 0.20 inferred from visibility.

To ensure that our transfer evaluation is reasonable, we further compare ground-network AOD with visibility-inferred AOD around the overpass time of MODIS. Selecting ground visibility sites within a radius of 0.25° of ground AOD sites leads to a difference below 0.01 between their mean AOD values; this criterion leads to 10 AOD sites with valid data for comparison. Loosening the distance criterion to 1.0° would include all AOD sites for comparison, which leads

to a negative mean bias of -0.05 in visibility-inferred AOD. These results support the use of ‘transfer evaluation’.

4.2. Spatial distribution

Fig. 5a–c compares the spatial distributions of annual average clear-sky AOD between MODIS/Terra and visibility-inferred data. As shown in Fig. 5a, MODIS/Terra AOD exceeds 0.5 at many stations in the North China Plain and Sichuan Basin due to large anthropogenic emissions of aerosols and precursors (Zhang et al., 2009; Wang et al., 2010). The high AOD in the Sichuan Basin is contributed also by the stagnant atmosphere trapping anthropogenic pollution (Li et al., 2003).

Fig. 5b shows that the visibility-inferred AOD roughly captures the general spatial pattern of MODIS/Terra AOD. Although smaller than MODIS/Terra AOD over the polluted North China Plain and Sichuan Basin, the visibility-inferred AOD exceeds MODIS/Terra values over the clean regions in the north (Fig. 5c). The scatter plot in Fig. 4b further shows that the annual mean visibility-inferred AOD are below 0.1 at much fewer stations than MODIS/Terra AOD. Overall, the spatial correlation between MODIS/Terra and visibility-inferred AOD reaches 0.58. The bias in the visibility-inferred AOD is negligible averaged across the stations, with a RMA regression slope of 0.93. Similar results are found for the comparisons between MODIS/Aqua AOD and respective visibility-inferred AOD (Figs. 4d and 6a–c).

An underestimate over the polluted North China Plain (Figs. 5c and 6c) means that the visibility-based AOD inference may underestimate the radiative forcing of aerosols over the region for 2006. Analysis of other years (e.g., since 2000 when MODIS data are available) can confirm whether the underestimate persists and how it may affect the long-term climatic forcings of aerosols. This can be done in our further study.

4.3. Seasonal distribution

Fig. 7 compares the seasonal variations of clear-sky AOD between MODIS and visibility-inferred datasets; the value for a given month represents the mean of all daily data in that month from all stations in East China. Both MODIS/Terra and MODIS/Aqua AOD peak in spring and early summer with a minimum value in winter, in general consistency with the seasonality shown in a previous study on CSHNET AOD (Wang et al., 2011). The visibility-inferred AOD captures the seasonal variability of MODIS AOD: the correlation coefficient exceeds 0.9 with respect to both Terra and Aqua. Regionally, the correlation is around 0.9 for polluted Northern East China encompassing 29° – 41°N and 110° – 123°E , and is about

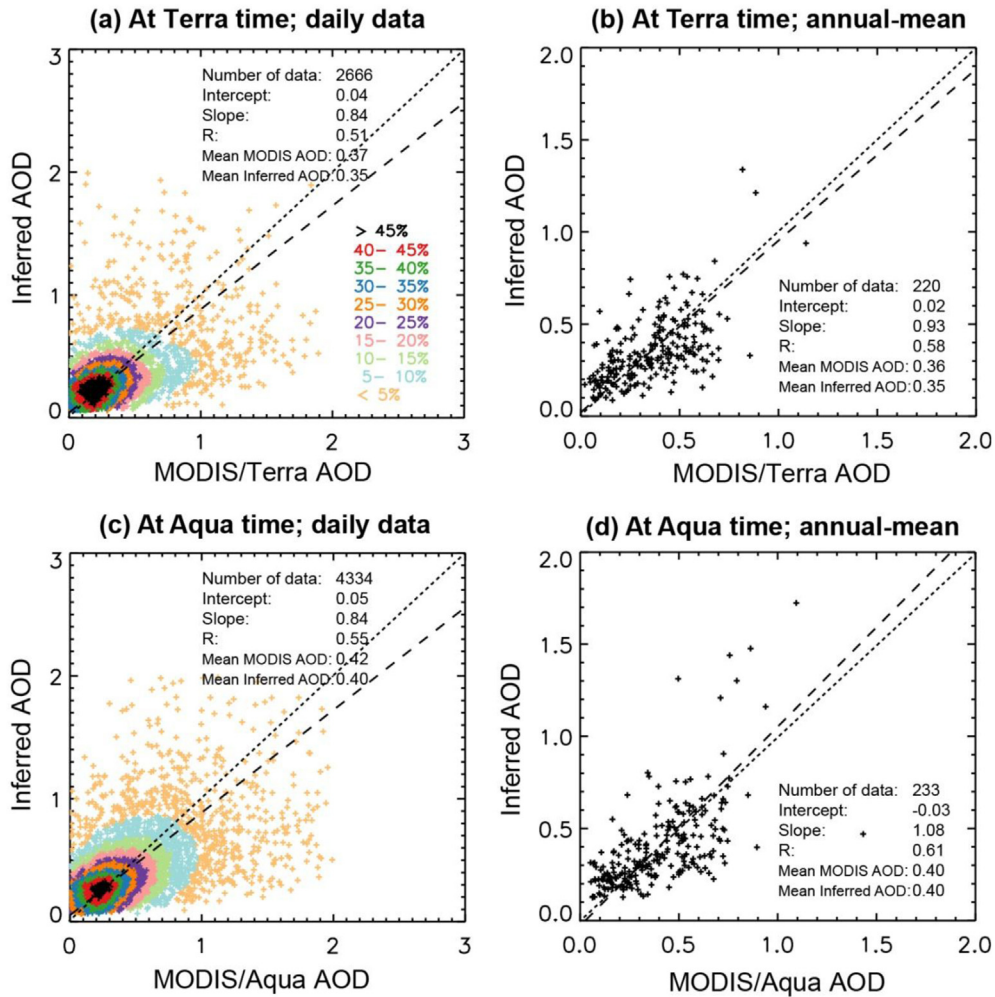


Fig. 4. Scatter plots of visibility-inferred AOD as a function of MODIS AOD over East China under cloud-free conditions. Each data pair in (a) and (c) represents a particular day at a particular station, while each data pair in (b) and (d) represents the annual mean value for a station. Colors in (a) and (c) and the percentages in (a) differentiate the number of data pairs within ± 0.2 of the AOD values of a given data pair, normalized to the total number of data pairs. The dashed line depicts the RMA regression and the dotted line indicates the 1:1 relationship. Also shown in each panel are number of data pairs, intercept and slope from the RMA regression, correlation coefficient, mean MODIS AOD, and mean visibility-inferred AOD. (For interpretation of the references to color in this figure legend, the reader is referred to the web version of this article.)

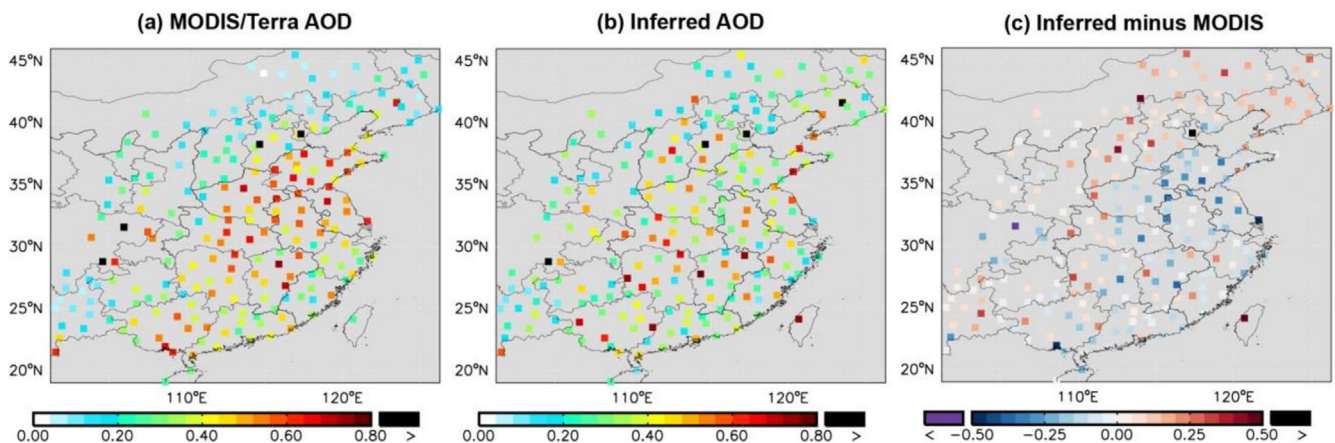


Fig. 5. Spatial distributions of (a) annual mean MODIS/Terra AOD, (b) respective visibility-inferred AOD, and (c) their differences over East China under cloud-free conditions.

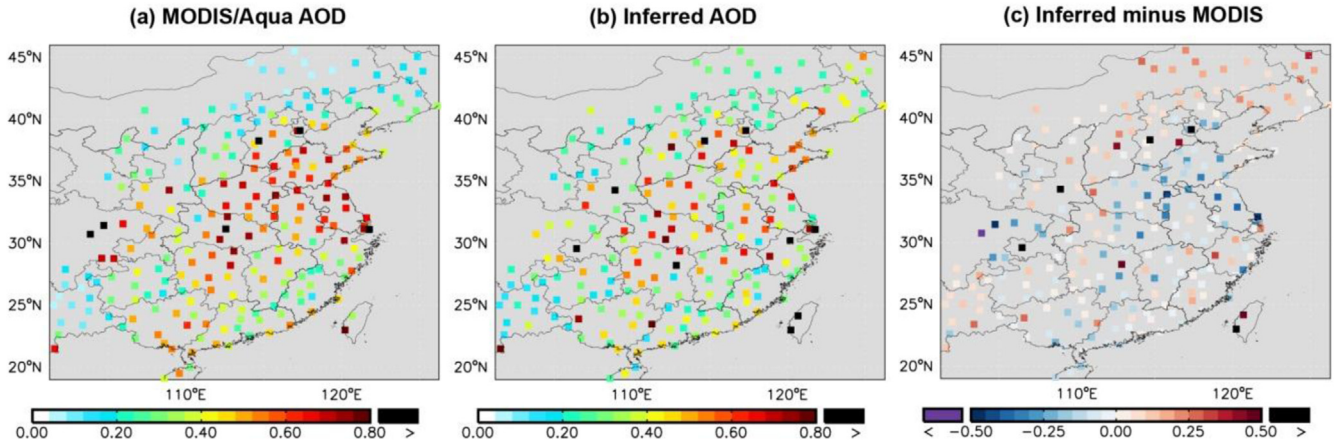


Fig. 6. Similar to Fig. 5 but for comparison with MODIS/Aqua.

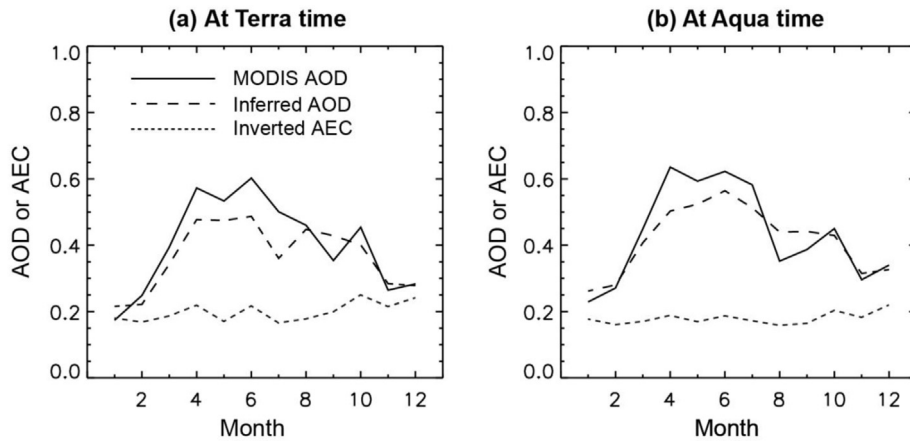


Fig. 7. Seasonal variations of MODIS AOD, visibility-inferred AOD and visibility-inverted AEC under cloud-free conditions averaged over all daily data at all stations in East China.

0.83–0.86 for the southern (south of 33°N) and northern (north of 33°N) areas of East China. Averaged over East China, the absolute difference between MODIS and visibility-inferred AOD is within 0.15 in any given month, with a relative difference within 30%. By comparison, the visibility-inverted AEC is relatively constant across the 12 months and does not correlate to MODIS AOD ($R < 0.10$ for both Terra and Aqua; Fig. 7).

4.4. Diurnal distribution

The solid black line in Fig. 8 presents the hourly variation of visibility-inferred AOD in the daytime under cloud-free conditions, averaged over all days and stations. A day and station is selected for analysis only when MODIS/Terra AOD, MODIS/Aqua AOD and respective visibility-inferred AOD data are all available. The visibility-inferred AOD reaches a maximum in the early morning with a minimum around midday. The range of daytime variation is about 0.12 (30% of daytime mean). A similar variation range (0.13, equal to 20% of daytime mean) is also found for ground-network AOD data despite their different spatiotemporal coverage. The inferred AOD data also capture the slight increase from the overpass time of Terra to Aqua shown in the MODIS datasets (from 0.348 to 0.366 in visibility-inferred AOD versus from 0.338 to 0.354 in MODIS data).

By comparison, the dashed black line in Fig. 8 shows the daytime variability of visibility-inverted AEC. The AEC peaks in the early

morning with subsequent reductions throughout the rest of the day. Its value at the overpass time of Terra is larger than the value at the overpass time of Aqua by 32%. The large difference in daytime variation between visibility-inverted AEC and visibility-inferred

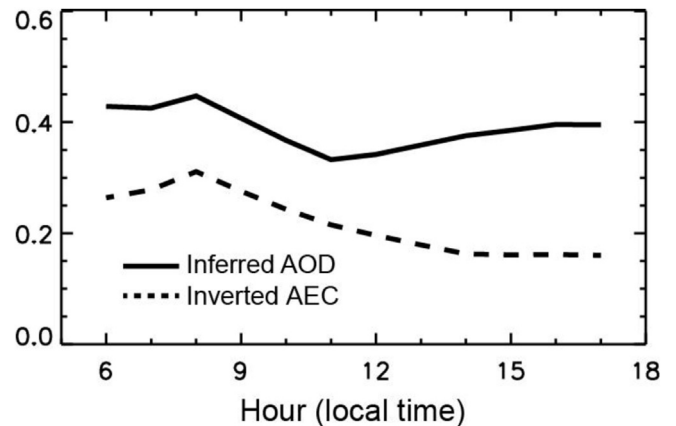


Fig. 8. Hourly variations of visibility-inferred AOD and visibility-inverted AEC in the daytime over East China under cloud-free conditions, averaged over all days and stations when and where MODIS/Terra AOD, MODIS/Aqua AOD and respective visibility-inferred AOD data are all available.

AOD is due to the temporally varying vertical distribution of aerosols simulated by GEOS-Chem.

5. Summary and discussion

This study uses near-surface visibility data measured every 3 h at ground meteorological stations to infer AOD over East China in 2006 under cloud-free conditions. We eliminate the optical effects of non-aerosol factors (air molecules and hydrometeors), convert visibility to near-surface aerosol extinction coefficient, and employ a GEOS-Chem simulation to relate columnar and near-surface aerosols in a spatiotemporally varying manner. We use MODIS Collection 5.1 AOD data retrieved from Terra and Aqua with strengthened data screening to evaluate the visibility-inferred AOD data, focusing on the spatial, seasonal and daytime hourly variations. MODIS AOD data are shown to be consistent with AOD data from three ground networks (AERONET, CARSNET and CSHNET) with a small negative bias of 0.05–0.08 and a RMA regression slope around unity.

Visibility-inferred AOD data roughly capture the general pattern of the frequency distribution of MODIS AOD, with a single mode at 0.1–0.2. Relative to both MODIS/Terra and MODIS/Aqua across all daily data from all stations, the inferred AOD have a mean bias within 0.02 and a correlation coefficient exceeding 0.5. Spatially, the annual mean inferred AOD correlates modestly to MODIS AOD (correlation is around 0.6), and it underestimates MODIS AOD over the polluted North China Plain.

The inferred AOD capture the seasonal variability of MODIS AOD with a correlation coefficient exceeding 0.9. They also reproduce the slight AOD increase from the late morning to the early afternoon suggested by the MODIS/Terra and MODIS/Aqua data. The well-reproduced temporal variability of AOD supports the use of the GEOS-Chem simulation in providing spatiotemporally varying columnar to near-surface relations for aerosols.

Routine visibility measurements from various ground stations have been demonstrated as a useful source of information for studying the long-term (e.g., interdecadal) variability of AOD and their climatic implications (Wang et al., 2009). In this study, the integration of 3-hourly visibility data and CTM simulations extends beyond previous studies employing daily mean or early afternoon visibility data along with simplified assumptions on the aerosol vertical profile. Extension of our analysis across the whole visibility time series (e.g., from 1973 to present) will improve our understanding of seasonal and daytime hourly variations in AOD and help inform the climatic impacts of aerosols. The spatial pattern of the inferred AOD should be improved.

Acknowledgments

This research is supported by the National Natural Science Foundation of China grant 41175127 and the 973 Project 2014CB441303. The work of Huizheng Che is supported by the NSFC grant 41275167 and the 973 Project 2014CB441201. Cimel master calibration of CARSNET was performed at the AERONET-EUROPE calibration center (LOA and AEMET-Tenerife), supported by ACT-RIS (European Union Seventh Framework Program (FP7/2007–2013) under grant agreement no. 262254).

We acknowledge the free use of MODIS aerosol and surface reflectance data from NASA, AOD measurements from AERONET, and visibility and ancillary meteorological data from NOAA NCDC.

References

Alexander, B., Park, R.J., Jacob, D.J., Li, Q.B., Yantosca, R.M., Savarino, J., Lee, C.C.W., Thiemens, M.H., 2005. Sulfate formation in sea-salt aerosols: constraints from

- oxygen isotopes. *J. Geophys. Res. Atmos.* 110, D10307. <http://dx.doi.org/10.1029/2004jd005659>.
- Che, H., Xia, X., Zhu, J., Li, Z., Dubovic, O., Holben, B., Goloub, P., Chen, H., Estelles, V., Cuevas-Agulló, E., Blarel, L., Wang, H., Zhao, H., Zhang, X., Wang, Y., Sun, J., Tao, R., Zhang, X., Shi, G., 2013. Column aerosol optical properties and aerosol radiative forcing during a serious haze-fog month over North China Plain in 2013 based on ground-based sunphotometer measurements. *Atmos. Chem. Phys. Discuss.* 13, 29685–29720. <http://dx.doi.org/10.5194/acpd-13-29685-2013>.
- Che, H.Z., Zhang, X.Y., Chen, H.B., Damiri, B., Goloub, P., Li, Z.Q., Zhang, X.C., Wei, Y., Zhou, H.G., Dong, F., Li, D.P., Zhou, T.M., 2009. Instrument calibration and aerosol optical depth validation of the China aerosol remote sensing network. *J. Geophys. Res. Atmos.* 114. <http://dx.doi.org/10.1029/2008jd011030>.
- Chen, D., Wang, Y., McElroy, M.B., He, K., Yantosca, R.M., Le Sager, P., 2009a. Regional CO pollution and export in China simulated by the high-resolution nested-grid GEOS-Chem model. *Atmos. Chem. Phys.* 9, 3825–3839.
- Chen, L.-X., Zhang, B., Zhu, W.-Q., Zhou, X.-J., Luo, Y.-F., Zhou, Z.-J., He, J.-H., 2009b. Variation of atmospheric aerosol optical depth and its relationship with climate change in China east of 100 E over the last 50 years. *Theor. Appl. Climatol.* 96, 191–199.
- Chen, Y., Shi, R., Wang, C., Yuanyuan, C., Gao, W., 2013. Estimating aerosol optical depth based on regional optimized Peterson model. *J. Geo-Information Sci.* 15, 241–248 (in Chinese).
- CMA: QX/T 47–2007, 2007. Specifications for Surface Meteorological Observation Part 3: Measurement of Meteorological Visibility. China Meteorological Administration, Beijing (in Chinese).
- Doyle, M., Dorling, S., 2002. Visibility trends in the UK 1950–1997. *Atmos. Environ.* 36, 3161–3172.
- Drury, E., Jacob, D.J., Spurr, R.J.D., Wang, J., Shinozuka, Y., Anderson, B.E., Clarke, A.D., Dibb, J., McNaughton, C., Weber, R., 2010. Synthesis of satellite (MODIS), aircraft (ICARTT), and surface (IMPROVE, EPA-AQS, AERONET) aerosol observations over eastern North America to improve MODIS aerosol retrievals and constrain surface aerosol concentrations and sources. *J. Geophys. Res. Atmos.* 115, D14204. <http://dx.doi.org/10.1029/2009jd012629>.
- Elterman, L., 1970. Relationships between vertical attenuation and surface meteorological range. *Appl. Opt.* 9, 1804–1810.
- Fairlie, T.D., Jacob, D.J., Park, R.J., 2007. The impact of transpacific transport of mineral dust in the United States. *Atmos. Environ.* 41, 1251–1266. <http://dx.doi.org/10.1016/j.atmosenv.2006.09.048>.
- Ford, B., Heald, C.L., 2012. An A-train and model perspective on the vertical distribution of aerosols and CO in the Northern Hemisphere. *J. Geophys. Res. Atmos.* 117, D06211. <http://dx.doi.org/10.1029/2011jd016977>.
- Fountoukis, C., Nenes, A., 2007. ISORROPIA II: a computationally efficient thermodynamic equilibrium model for K^+ - Ca^{2+} - Mg^{2+} - NH_4^+ - Na^+ - SO_4^{2-} - NO_3^- - Cl^- - H_2O aerosols. *Atmos. Chem. Phys.* 7, 4639–4659.
- Griffing, G.W., 1980. Relations between the prevailing visibility, nephelometer scattering coefficient and sunphotometer turbidity coefficient. *Atmos. Environ.* (1967) 14, 577–584.
- Guenther, A., Karl, T., Harley, P., Wiedinmyer, C., Palmer, P., Geron, C., 2006. Estimates of global terrestrial isoprene emissions using MEGAN (Model of Emissions of Gases and Aerosols from Nature). *Atmos. Chem. Phys.* 6, 3181–3210.
- Holben, B.N., Eck, T.F., Slutsker, I., Tanre, D., Buis, J.P., Setzer, A., Vermote, E., Reagan, J.A., Kaufman, Y.J., Nakajima, T., Lavenu, F., Jankowiak, I., Smirnov, A., 1998. AERONET – a federated instrument network and data archive for aerosol characterization. *Remote Sens. Environ.* 66, 1–16.
- Husar, R.B., Husar, J.D., Martin, L., 2000. Distribution of continental surface aerosol extinction based on visual range data. *Atmos. Environ.* 34, 5067–5078.
- Hyer, E.J., Reid, J.S., Zhang, J., 2011. An over-land aerosol optical depth data set for data assimilation by filtering, correction, and aggregation of MODIS collection 5 optical depth retrievals. *Atmos. Meas. Tech.* 4, 379–408. <http://dx.doi.org/10.5194/amt-4-379-2011>.
- Ichoku, C., Remer, L.A., Eck, T.F., 2005. Quantitative evaluation and intercomparison of morning and afternoon MODIS aerosol measurements from the Terra and Aqua satellites. *J. Geophys. Res.* 110.
- Jaeglé, L., Quinn, P.K., Bates, T.S., Alexander, B., Lin, J.T., 2011. Global distribution of sea salt aerosols: new constraints from in situ and remote sensing observations. *Atmos. Chem. Phys.* 11, 3137–3157. <http://dx.doi.org/10.5194/acp-11-3137-2011>.
- Kaufman, Y.J., Holben, B.N., Tanré, D., Slutsker, I., Smirnov, A., Eck, T.F., 2000. Will aerosol measurements from Terra and Aqua polar orbiting satellites represent the daily aerosol abundance and properties? *Geophys. Res. Lett.* 27, 3861–3864.
- Kessner, A.L., Wang, J., Levy, R.C., Colarco, P.R., 2013. Remote sensing of surface visibility from space: a look at the United States East Coast. *Atmos. Environ.* 81, 136–147.
- Lamsal, L.N., Martin, R.V., van Donkelaar, A., Steinbacher, M., Celarier, E.A., Bucsela, E., Dunlea, E.J., Pinto, J.P., 2008. Ground-level nitrogen dioxide concentrations inferred from the satellite-borne ozone monitoring instrument. *J. Geophys. Res. Atmos.* 113, D16308. <http://dx.doi.org/10.1029/2007jd009235>.
- Levy, R.C., Remer, L.A., Mattoo, S., Vermote, E.F., Kaufman, Y.J., 2007. Second – generation operational algorithm: retrieval of aerosol properties over land from inversion of moderate resolution imaging spectroradiometer spectral reflectance. *J. Geophys. Res. Atmos.* (1984–2012) 112.
- Li, C., Mao, J., Lau, K.-H.A., Chen, J.-C., Yuan, Z., Liu, X., Zhu, A., Liu, G., 2003. Characteristics of distribution and seasonal variation of aerosol optical depth in eastern China with MODIS products. *Chin. Sci. Bull.* 48, 2488–2495.

- Li, Z.Q., Niu, F., Lee, K.H., Xin, J.Y., Hao, W.M., Nordgren, B., Wang, Y.S., Wang, P.C., 2007. Validation and understanding of moderate resolution imaging spectroradiometer aerosol products (C5) using ground-based measurements from the handheld Sun photometer network in China. *J. Geophys. Res. Atmos.* 112 <http://dx.doi.org/10.1029/2007jd008479>.
- Lin, J.-T., 2012. Satellite constraint for emissions of nitrogen oxides from anthropogenic, lightning and soil sources over East China on a high-resolution grid. *Atmos. Chem. Phys.* 12, 2881–2898. <http://dx.doi.org/10.5194/acp-12-2881-2012>.
- Lin, J.-T., McElroy, M.B., 2010. Impacts of boundary layer mixing on pollutant vertical profiles in the lower troposphere: implications to satellite remote sensing. *Atmos. Environ.* 44, 1726–1739. <http://dx.doi.org/10.1016/j.atmosenv.2010.02.009>.
- Lin, J.-T., McElroy, M.B., 2011. Detection from space of a reduction in anthropogenic emissions of nitrogen oxides during the Chinese economic downturn. *Atmos. Chem. Phys.* 11, 8171–8188. <http://dx.doi.org/10.5194/acp-11-8171-2011>.
- Lin, J.-T., Youn, D., Liang, X.-Z., Wuebbles, D.J., 2008. Global model simulation of summertime U.S. ozone diurnal cycle and its sensitivity to PBL mixing, spatial resolution, and emissions. *Atmos. Environ.* 42, 8470–8483. <http://dx.doi.org/10.1016/j.atmosenv.2008.08.012>.
- Lin, J.-T., McElroy, M.B., Boersma, K.F., 2010. Constraint of anthropogenic NO_x emissions in China from different sectors: a new methodology using multiple satellite retrievals. *Atmos. Chem. Phys.* 10, 63–78.
- Lin, J.-T., Liu, Z., Zhang, Q., Liu, H., Mao, J., Zhuang, G., 2012. Modeling uncertainties for tropospheric nitrogen dioxide columns affecting satellite-based inverse modeling of nitrogen oxides emissions. *Atmos. Chem. Phys.* 12, 12255–12275. <http://dx.doi.org/10.5194/acp-12-12255-2012>.
- Lin, J.-T., Martin, R.V., Boersma, K.F., Snee, P., Stammes, P., Spurr, R., Wang, P., Van Roozendaal, M., Clémer, K., Irie, H., 2014. Retrieving tropospheric nitrogen dioxide from the ozone monitoring instrument: effects of aerosols, surface reflectance anisotropy, and vertical profile of nitrogen dioxide. *Atmos. Chem. Phys.* 14, 1441–1461. <http://dx.doi.org/10.5194/acp-14-1441-2014>.
- Liu, H., Jacob, D.J., Bey, I., Yantosca, R.M., 2001. Constraints from ²¹⁰Pb and ⁷Be on wet deposition and transport in a global three-dimensional chemical tracer model driven by assimilated meteorological fields. *J. Geophys. Res.* 106, 12109–12112, 12128.
- Liu, J., Xia, X., Wang, P., Li, Z., Zheng, Y., Cribb, M., Chen, H., 2007. Significant aerosol direct radiative effects during a pollution episode in northern China. *Geophys. Res. Lett.* 34, L23808. <http://dx.doi.org/10.1029/2007gl030953>.
- Liu, Y., Wang, Z., Wang, J., Ferrare, R.A., Newsom, R.K., Welton, E.J., 2011. The effect of aerosol vertical profiles on satellite-estimated surface particle sulfate concentrations. *Remote Sens. Environ.* 115, 508–513.
- Lott, N., 2004. The quality control of the integrated surface hourly database. In: 84th American Meteorological Society Annual Meeting, Seattle, WA.
- Mi, W., Li, Z., Xia, X., Holben, B., Levy, R., Zhao, F., Chen, H., Cribb, M., 2007. Evaluation of the moderate resolution imaging spectroradiometer aerosol products at two aerosol robotic network stations in China. *J. Geophys. Res.* 112, D22S08.
- Murray, L.T., Jacob, D.J., Logan, J.A., Hudman, R.C., Koshak, W.J., 2012. Optimized regional and interannual variability of lightning in a global chemical transport model constrained by LIS/OTD satellite data. *J. Geophys. Res. Atmos.* 117, D20307. <http://dx.doi.org/10.1029/2012jd017934>.
- Ott, L.E., Pickering, K.E., Stenchikov, G.L., Allen, D.J., DeCaria, A.J., Ridley, B., Lin, R.-F., Lang, S., Tao, W.-K., 2010. Production of lightning NO(x) and its vertical distribution calculated from three-dimensional cloud-scale chemical transport model simulations. *J. Geophys. Res. Atmos.* 115, D04301. <http://dx.doi.org/10.1029/2009jd011880>.
- Pan, L., Che, H., Geng, F., Xia, X., Wang, Y., Zhu, C., Chen, M., Gao, W., Guo, J., 2010. Aerosol optical properties based on ground measurements over the Chinese Yangtze Delta Region. *Atmos. Environ.* 44, 2587–2596. <http://dx.doi.org/10.1016/j.atmosenv.2010.04.013>.
- Park, R.J., Jacob, D.J., Chin, M., Martin, R.V., 2003. Sources of carbonaceous aerosols over the United States and implications for natural visibility. *J. Geophys. Res. Atmos.* 108, 4355. <http://dx.doi.org/10.1029/2002jd003190>.
- Park, R.J., Jacob, D.J., Field, B.D., Yantosca, R.M., Chin, M., 2004. Natural and transboundary pollution influences on sulfate-nitrate-ammonium aerosols in the United States: implications for policy. *J. Geophys. Res. Atmos.* 109, D15204. <http://dx.doi.org/10.1029/2003jd004473>.
- Price, C., Penner, J., Prather, M., 1997. NO_x from lightning, 1, global distribution based on lightning physics. *J. Geophys. Res.* 102, 12. <http://dx.doi.org/10.1029/96JD03504>.
- Qian, Y., Giorgi, F., 2000. Regional climatic effects of anthropogenic aerosols? the case of Southwestern China. *Geophys. Res. Lett.* 27, 3521–3524.
- Qian, Y., Gong, D., Fan, J., Leung, L.R., Bennartz, R., Chen, D., Wang, W., 2009. Heavy pollution suppresses light rain in China: observations and modeling. *J. Geophys. Res. Atmos.* (1984–2012) 114, D00K02. <http://dx.doi.org/10.1029/2008JD011575>.
- Qin, S., Shi, G., Chen, L., Wang, B., Zhao, J., Yu, C., Shu, Y., 2010. Long-term variation of aerosol optical depth in china based on meteorological horizontal visibility observations. *Chin. J. Atmos. Sci.* 34, 449–456.
- Qiu, J., Lin, Y., 2001. A parameterization model of aerosol optical depths in China. *Acta Meteorol. Sin.* 59, 368–372 (in Chinese).
- Rienecker, M.M., Suarez, M.J., Todling, R., Bacmeister, J., Takacs, L., Liu, H.-C., Gu, W., Sienkiewicz, M., Koster, R.D., Gelaro, R., Stajner, I., Nielsen, E., 2008. The GEOS-5 Data Assimilation System – Documentation of Versions 5.0.1, 9.1.0, and 5.2.0. NASA.
- Smirnov, A., Holben, B., Eck, T., Dubovik, O., Slutsker, I., 2000. Cloud-screening and quality control algorithms for the AERONET database. *Remote Sens. Environ.* 73, 337–349. [http://dx.doi.org/10.1016/S0034-4257\(00\)00109-7](http://dx.doi.org/10.1016/S0034-4257(00)00109-7).
- Smith, A., Lott, N., Vose, R., 2011. The integrated surface database: recent developments and partnerships. *Bull. Am. Meteorol. Soc.* 92.
- Streets, D.G., Bond, T.C., Carmichael, G.R., Fernandes, S.D., Fu, Q., He, D., Klimont, Z., Nelson, S.M., Tsai, N.Y., Wang, M.Q., Woo, J.H., Yarber, K.F., 2003. An inventory of gaseous and primary aerosol emissions in Asia in the year 2000. *J. Geophys. Res. Atmos.* 108, 8809. <http://dx.doi.org/10.1029/2002jd003093>.
- Tao, R., Che, H., Chen, Q., Wang, Y., Sun, J., Zhang, X., Lu, S., Guo, J., Wang, H., Zhang, X., 2013. Development of an integrating sphere calibration method for Cimel sunphotometers in China aerosol remote sensing network. *Particulate. Environ. Sci.* <http://dx.doi.org/10.1016/j.partic.2013.04.009>.
- van der Werf, G.R., Randerson, J.T., Giglio, L., Collatz, G.J., Kasibhatla, P.S., Arellano, A.F., 2006. Interannual variability in global biomass burning emissions from 1997 to 2004. *Atmos. Chem. Phys.* 6, 3423–3441.
- van Donkelaar, A., Martin, R.V., Brauer, M., Kahn, R., Levy, R., Verduzco, C., Villeneuve, P.J., 2010. Global estimates of ambient fine particulate matter concentrations from satellite-based aerosol optical depth: development and application. *Environ. Health Perspect.* 118, 847–855.
- van Donkelaar, A., Martin, R.V., Spurr, R.J.D., Drury, E., Remer, L.A., Levy, R.C., Wang, J., 2013. Optimal estimation for global ground-level fine particulate matter concentrations. *J. Geophys. Res. Atmos.* 118, 5621–5636. <http://dx.doi.org/10.1002/jgrd.50479>.
- Vautard, R., Yiou, P., van Oldenborgh, G.J., 2009. Decline of fog, mist and haze in Europe over the past 30 years. *Nat. Geosci.* 2, 115–119.
- Wang, K., Dickinson, R., Su, L., Trenberth, K., 2012. Contrasting trends of mass and optical properties of aerosols over the Northern Hemisphere from 1992 to 2011. *Atmos. Chem. Phys.* 12, 9387–9398. <http://dx.doi.org/10.5194/acp-12-9387-2012>.
- Wang, K.C., Dickinson, R.E., Liang, S.L., 2009. Clear sky visibility has decreased over land globally from 1973 to 2007. *Science* 323, 1468–1470. <http://dx.doi.org/10.1126/science.1167549>.
- Wang, L., Wang, Y., Xin, J., Li, Z., Wang, X., 2010. Assessment and comparison of three years of Terra and Aqua MODIS Aerosol Optical Depth Retrieval (C005) in Chinese terrestrial regions. *Atmos. Res.* 97, 229–240.
- Wang, L.L., Xin, J.Y., Wang, Y.S., Li, Z.Q., Liu, G.R., Li, J., 2007. Evaluation of the MODIS aerosol optical depth retrieval over different ecosystems in China during EAST-AIRE. *Atmos. Environ.* 41, 7138–7149. <http://dx.doi.org/10.1016/j.atmosenv.2007.05.001>.
- Wang, Y., Jacob, D.J., Logan, J.A., 1998. Global simulation of tropospheric O₃-NO_x-hydrocarbon chemistry, 1. Model formulation. *J. Geophys. Res.* 103, 10713–10725.
- Wang, Y., Xin, J., Li, Z., Wang, S., Wang, P., Hao, W.M., Nordgren, B.L., Chen, H., Wang, L., Sun, Y., 2011. Seasonal variations in aerosol optical properties over China. *J. Geophys. Res. Atmos.* (1984–2012) 116.
- Wesely, M.L., 1989. Parameterization of surface resistances to gaseous dry deposition in regional-scale numerical-models. *Atmos. Environ.* 23, 1293–1304.
- WMO, 2008. Guide to Meteorological Instruments and Methods of Observation. World Meteorological Organization.
- Xie, Y., Zhang, Y., Xiong, X., Qu, J.J., Che, H., 2011. Validation of MODIS aerosol optical depth product over China using CARSNET measurements. *Atmos. Environ.* 45, 5970–5978.
- Xin, J., Wang, L., Wang, Y., Li, Z., Wang, P., 2011. Trends in aerosol optical properties over the Bohai Rim in Northeast China from 2004 to 2010. *Atmos. Environ.* 45, 6317–6325.
- Xin, J.Y., Wang, Y.S., Li, Z.Q., Wang, P.C., Hao, W.M., Nordgren, B.L., Wang, S.G., Liu, G.R., Wang, L.L., Wen, T.X., Sun, Y., Hu, B., 2007. Aerosol optical depth (AOD) and Angstrom exponent of aerosols observed by the Chinese Sun Hazemeter Network from August 2004 to September 2005. *J. Geophys. Res. Atmos.* 112 <http://dx.doi.org/10.1029/2006jd007075>.
- Yang, D., Li, C., Lau, A.K.H., Li, Y., 2013. Long-term measurement of daytime atmospheric mixing layer height over Hong Kong. *J. Geophys. Res. Atmos.* 118, 2422–2433. <http://dx.doi.org/10.1002/jgrd.50251>.
- Yienger, J.J., Levy, H., 1995. Empirical model of global soil-biogenic NO_x emissions. *J. Geophys. Res.* 100, 11447–11464.
- Zhang, Q., Streets, D.G., Carmichael, G.R., He, K.B., Huo, H., Kannari, A., Klimont, Z., Park, I.S., Reddy, S., Fu, J.S., Chen, D., Duan, L., Lei, Y., Wang, L.T., Yao, Z.L., 2009. Asian emissions in 2006 for the NASA INTEX-B mission. *Atmos. Chem. Phys.* 9, 5131–5153.
- Zhao, Y., Duan, L., Xing, J., Larssen, T., Nielsen, C.P., Hao, J.M., 2009. Soil acidification in China: is controlling SO₂ emissions enough? *Environ. Sci. Technol.* 43, 8021–8026. <http://dx.doi.org/10.1021/es901430n>.
- Zhu, Z., Yu, J., Gong, W., 2011. Parameter selection and optimization of Peterson model. *Geomatics Inf. Sci. Wuhan Univ.* 36, 1025–1029 (in Chinese).